Observations of 5.9 GHz radio propagation and 802.11p network performance at road junctions

C.J. Clayton[1]*, A.J. Stocker[1], S.K.A. Alwane[1], and D. Hassan[1]

[1] Department of Engineering, University of Leicester, U.K.

Corresponding author: Alan Stocker (sto@leicester.ac.uk)

*Now at SNC Lavalin's Atkins Business, Manchester, U.K.

Key Points:

- Observations of 802.11p performance at road junctions indicate that reliable communication can be expected at ranges of 45–70 m
- In 70% of cases, the presence of vehicles marginally improves network performance
- An empirical relationship between received signal strength and network performance is presented

Abstract

The propagation of 5.9 GHz radio signals and performance of an 802.11p network were measured at three road junctions each having a different density of buildings. The maximum range for which acceptable performance (defined as where the packet delivery ratio was greater than 90%) was dependent on the junction but lay in the range of 45–70 m. While reflections from transient vehicles were often found to have a small positive impact on network performance, this could not be relied upon to provide a reliable improvement in communications. The received signal strength was dependent on the junction type with the strong reflections from buildings located on the opposite side of a T-junction leading to higher signal strength. Finally, an empirical relationship between the packet delivery ratio and the received signal strength has been established that will allow modelers to link signal strength to network performance for field conditions.

1 Introduction

Vehicle-to-vehicle (V2V) and vehicle-to-infrastructure (V2I) communications (collectively known as V2X) are important components of the drive towards connected and autonomous vehicles. An additional 75 MHz of spectrum, named the Dedicated Short-Range Communications (DSRC) band, has been allocated at 5.9 GHz in some countries (e.g. USA, UK, Germany and Australia) with the purpose of implementing connected Intelligent Transport Systems (ITS). Initially, and at the time of the experiments reported in this paper being conducted, this band was to be used solely by IEEE 802.11p networks but now the DSRC band might also be used by Cellular-V2X (C-V2X) networks (also known as LTE-V, Long Term Evolution for Vehicles). It is yet to be decided by governments or standardizing bodies if the DSRC band will be exclusively reserved for just one of these networks or if it will be shared by both technologies – a decision that will be reached with further evolution of the 5G (IMT-2020) standard of which C-V2X will form a part. Irrespective of which technology gets to use the DSRC band, the propagation data presented in this paper remains important since it will be valuable to both Radio Access Technologies (RATs) whilst the network performance data will be useful in comparisons against C-V2X networks implemented in similar environments.

The performance of V2X systems (e.g. IEEE 801.11p/ITS-G5) depends on the propagation environment. For example, in motorway driving the propagation path is relatively uncluttered and ranges are many hundreds of metres (Paier et al., 2010), while in the urban environment, the range will typically be less than 50 m (e.g. see Meireles et al, 2010) because of the presence of buildings. Some of the propagation modes that can occur in the urban environment are illustrated in Figure 1. For safety critical systems (e.g. collision avoidance), the shorter propagation ranges result in shorter timescales for drivers (human or machine) to react. Mangel et al. (2011), completed an extensive survey of the effect of a number of road junctions and developed a parameterized empirical model (virtualsource11p) of the signal path loss at regular shaped junctions with buildings at each corner as follows.

$$virtualsource11p(d_r, d_t\ w_r, x_t, i_s) = 3.75 + \ 2.94 i_s + \begin{cases} 10\log_{10}\left(\left(\frac{d_t^{0.957}}{(x_t w_r)^{0.81}}\frac{4\pi d_r}{\lambda}\right)^{2.69}\right), & d_r \le d_b \\ 10\log_{10}\left(\left(\frac{d_t^{0.957}}{(x_t w_r)^{0.81}}\frac{4\pi d_r^2}{\lambda}\right)^{2.69}\right), & d_r > d_b \end{cases} \quad (1)$$

Where d_r and d_t are the distances from the receiver and transmitter to the intersection center, respectively, w_r is the width of the street in which the receiver is located, x_t is the distance from the transmitter to the building wall on the same side as the receiver, d_b is the breakpoint distance ($\approx 4h_t h_r/\lambda$, where h_t and h_r are the height of the antennas at the transmitter and receiver, respectively), λ is the wavelength (0.0508 m for the DSRC band), and i_s is the sub-urban loss factor (which is 0 or 1 for urban and suburban conditions, respectively). This model is valid for d_r>10 m,

and has been derived from measurements where w_r>20 m, $w_r \approx w_t$ (where w_t is the width of the street in which the transmitter is located) and d_t>30 m. Other experimental measurements have been reported (e.g. Abbas et al., 2013; Alexander et al, 2011; Cheng et al., 2007b; Schumacher et al., 2012) and path loss models developed (e.g. Sommer et al., 2011; Tchouankem et al., 2015). The model of Sommer et al. (2011) accounts for the shadowing and penetration effects of buildings with a pass loss given by

$$P_L = 10\log_{10}\left(\frac{\lambda^2}{16\pi^2 d^\alpha}\right) + \beta n + \gamma d_m \quad (2)$$

Where, d is the direct distance between transmitter and receiver, α=2.2, β is the attenuation due to the external wall of a building, n is the number of walls traversed, γ is the specific attenuation inside buildings, and d_m is the total distance that the direct path lies within buildings. Sommer et al. (2011) found that standard values of $\beta \approx 9$ dB and $\gamma \approx 0.4$ dB/m fitted the majority of their experimental data, but that for some buildings other values of β and γ gave a better fit. While there are a number of approaches to calculating the effects of diffraction, a relatively straightforward method for finding the loss due to knifeedge diffraction is described in ITU-R (2018).

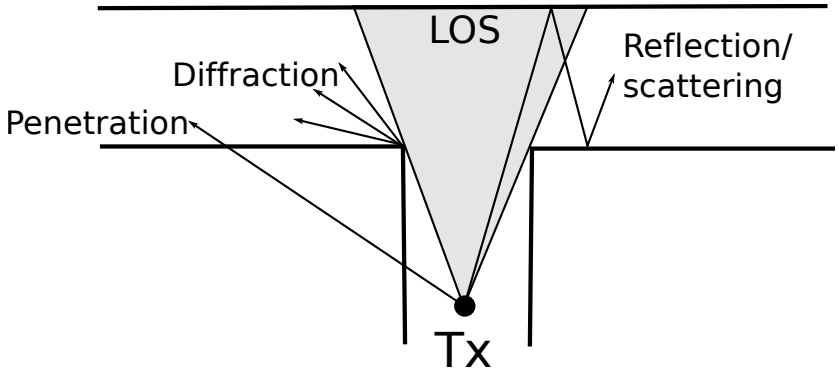

Figure 1. A schematic of the likely propagation modes found in the urban environment. Depending on their construction, the signal can also propagate through the buildings

Empirical models of the type described above (e.g. Mangel et al., 2011) have the benefit of being computationally light and relatively easy to apply to digital maps. Typically they provide median loss values with the possibility of adding the effect of signal fading via statistical models. The weakness of such models is that they are dependent on the range of situations for which measurements have been obtained and used to derive the model (e.g. Mangel et al., 2011 used measurements from ten junctions in Munich) and that the number of parameters included in the model is, necessarily, limited. Alternatively, a physics-based, e.g. raytracing, approach can be used to determine the received signal power (and also delay and Doppler spread). This method relies on a detailed description of the propagation environment (e.g. building locations) and can be highly computationally intensive when applied to network simulations, although methods have been developed to improve performance (Pilosu et al., 2011). Information about some elements of the propagation environment are more difficult to obtain, e.g. street furniture is likely to cause scattering, reflection and transmission coefficients will depend on building materials, and vegetation will cause additional loss. This level of detail is not routinely included on maps and can, therefore, be difficult to include in modelling but may have significant impact on the outcomes. Finally, the vehicles themselves will also have a strong influence on the propagation.

In this paper, we present experimental measurements of the signal strength and network performance of an 802.11p network for three T-junctions varying in how built-up they were. Of these junctions, one has buildings on all sides (Junction A), one is a relatively open junction with only one building (Junction C), while the third falls between these two extremes (Junction B). The measurements show that virtualsource11p predicts the signal strength very well for Junctions B and

C, but poorly for Junction A. The maximum effective range where reliable communications can occur (which strongly impacts on the time available for collision avoidance) has also been derived from the measurements and, at 45–70 m, this is consistent with observations reported by Meireles et al. (2010) and Schumacher et al (2012). In addition, the behavior of the packet delivery ratio (PDR) with received signal strength was also characterized, which enables network performance to be estimated from the signal strength.

2 Method

A measurement system similar to that used by Cheng et al. (2007a) consisting of an 802.11p network system (NS) and a continuous wave system (CWS) was used to simultaneously measure network performance and channel parameters (signal strength and Doppler), respectively at three T-junctions. The antennas for the CWS and NS were placed a distance of 0.508 m apart (corresponding to ten wavelengths at 5.9 GHz), on a wooden plane situated 1 m above ground level and placed on a wooden, wheeled cart. This offset between the antennas means that the propagation path for the CWS signal was slightly different to that of the NS signal. However, the difference in measurements obtained with the antenna positions swapped was small compared to the level of fading and therefore this can be neglected.

2.1 Continuous wave system (CWS)

The CWS used a signal generator to produce a 5.9 GHz CW signal with an EIRP of 16 dBm (i.e. the transmitted power was 10 dBm and the antenna gain 6 dB). This is consistent with the transmit powers used in some other experiments (e.g. Cheng et al., 2007a; Meireles et al., 2010), but is below the maximum transmit power of 23 or 33 dBm (this depends on the channel and whether the system is classed as private or public) allowed by the 802.11p standard. The omnidirectional antennas used at the transmitter and receiver each had a gain of 6 dBi. The spectrum of the received signal was measured using a spectrum analyzer with a span set to 500 Hz. This meant that the Doppler shifts caused by traffic (up to speeds of approximately 13 ms^{-1}) could be measured. Each spectrum was time-stamped and saved to disk at intervals of, on average, 1.5 s (the standard deviation in the time interval was ~ 0.3 s). Thirty spectra were usually collected at each location (i.e. over a period of approximately 45 s) allowing statistically valid measurements to be made. Occasionally, the spectrum analyzer underwent auto calibration and consequently a few spectra were not recorded.

Two example spectra displaying different Doppler spread characteristics are presented in Figure 2. The signal strength values presented in this paper are derived from the peak power in the measured spectra. The Doppler spread, f_D is calculated from the range of frequencies where the signal is above the noise floor (taken as −111 dBm for the collected spectra). Figure 3 shows an example of the signal power for the 30 spectra collected at a single location. During this interval, the median peak power (MPP) is −68.5 dBm with upper and lower deciles of −66.9 and −73.0 dBm, respectively. While the peak in the spectrum remains fairly fixed in frequency, the sidebands, which are more than 10 dB weaker than the peak, vary in frequency indicating the presence of a moving object affecting the signal. During the experiments, the presence and type (i.e. vehicular or pedestrian) of traffic was noted manually but, unfortunately, the records were not always complete. Typically, the peak power is affected by the passage of the vehicle by less than 5 dB. In this example, removing the spectra where the vehicle was present (for this purpose assumed to be where f_D>50 Hz) from the calculation of the MPP changes the value to −70.2 dBm. This change of 1.7 dB in MPP is typical of cases where traffic has affected the spectra, is smaller than the fading, and therefore spectra affected by traffic have not been excluded from the calculation of MPP.

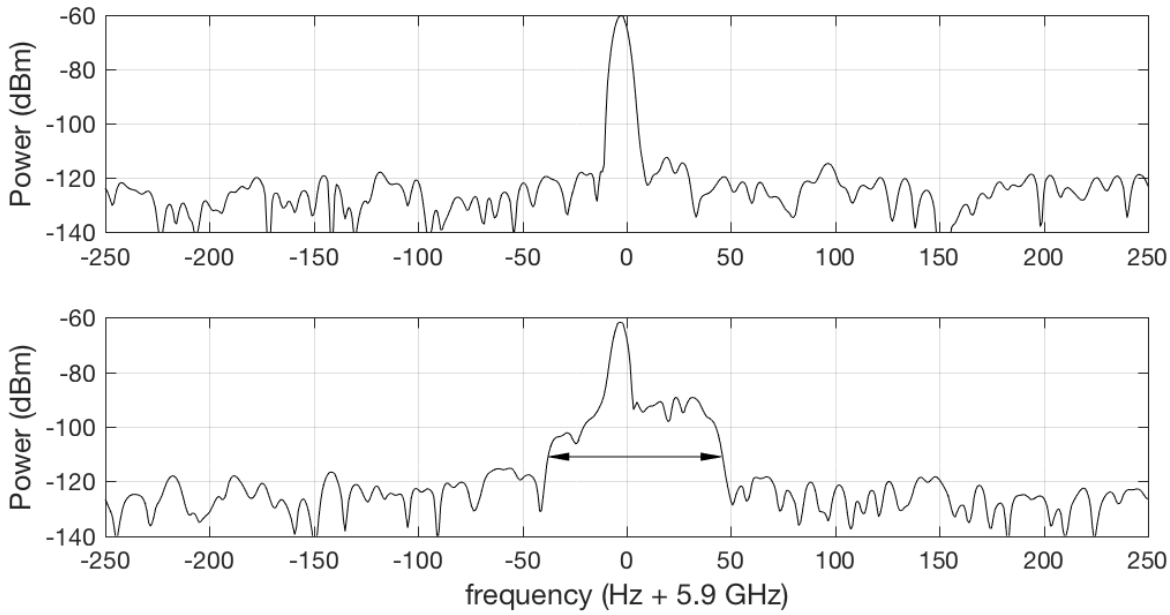

Figure 2. Two spectra obtained at a distance of +8 m from Junction A. In the bottom panel, a passing vehicle (travelling at ~3 ms^{-1}) affects the spectrum. In the bottom panel, the arrows indicate the Doppler spread (17 Hz and 83 Hz in the top and bottom panels, respectively).

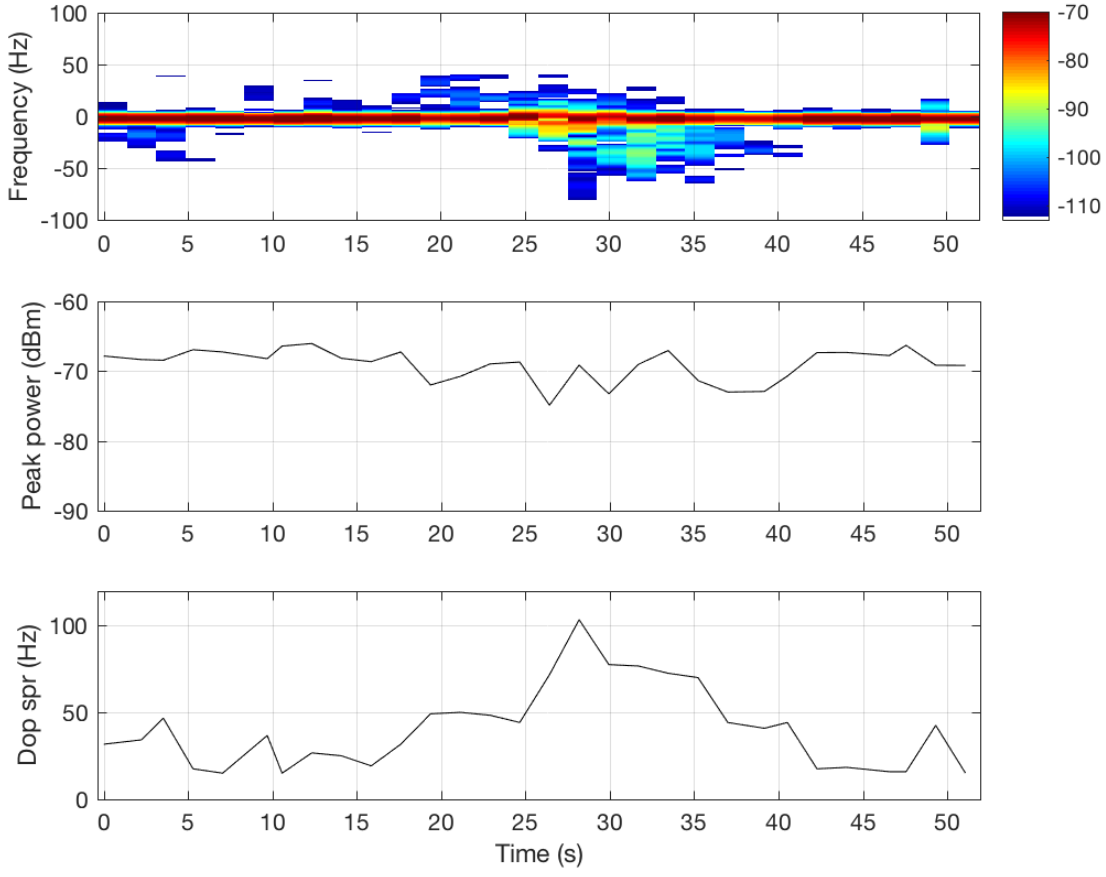

Figure 3. (top panel) Signal spectrum, (middle panel) peak signal power, and (lower panel) Doppler spread as a function of time measured at a distance of +6 m from Junction A. The color scale indicates received signal power (in dBm).

2.2 Network system (NS)

The NS consisted of two NEC Linkbirds (version 4), one operating as a transmitter and the other as a receiver over virtually the same path as the CWS (the only difference being the 10

wavelength offset between the antennas) with identical transmit power and antennas. The packet size was 250 bytes, while the data rate of 6 Mbps followed Jiang et al. (2008) who found that this gave the highest Packet Delivery Ratio (PDR). A packet, which consisted of a time stamp, a unique packet number, and a collection of random numbers with a checksum, was emitted by the transmitter every 0.1 s. The time that each packet arrived at the receiver was recorded along with the RSSI. However, the clocks at the NS transmitter and receiver were not synchronized and this meant that the packet delivery time (or delay time) could not be reliably determined. Given that this was a single hop link, this is not likely to have varied much in any case. The clocks for the CWS and NS were also not synchronized and occasionally a few packets were received before the first spectrum and after the last spectrum leading to an observed PDR>100%. In these cases, the plotted PDR was capped at 100%. While the RSSI of the NS could be used to measure the signal strength, the spectrum analyzer has been calibrated and is capable of measuring the signal strength in cases where no, or few, packets are received.

2.3 Experimental arrangement

Measurements of signal strength and PDR have been collected at three T-junctions differentiated by the degree to which buildings are present at the junction with some similarity to the locations used by Mangel et al. (2011). Junction A (Figure 4) has narrow roads (single lanes) and buildings on all sides of the junctions, Junction B (Figure 5) has dual lane roads and fewer buildings, while Junction C (Figure 6) consists of wide roads and only one building. For Junction C, the road slopes downwards as the distance increases from the center of the intersection with a drop of about 2 m in 70 m. Measurements made at Junction A were only affected by pedestrian and cycle traffic since motorized vehicles were asked to wait while data were collected, whereas pedestrians, cyclists and vehicles were present at the other two junctions. In addition, the road along which the receiver was moved for Junction C was a public road and this meant that there was a higher occurrence of larger and faster vehicles than for the other junctions and the presence of vehicles was not recorded.

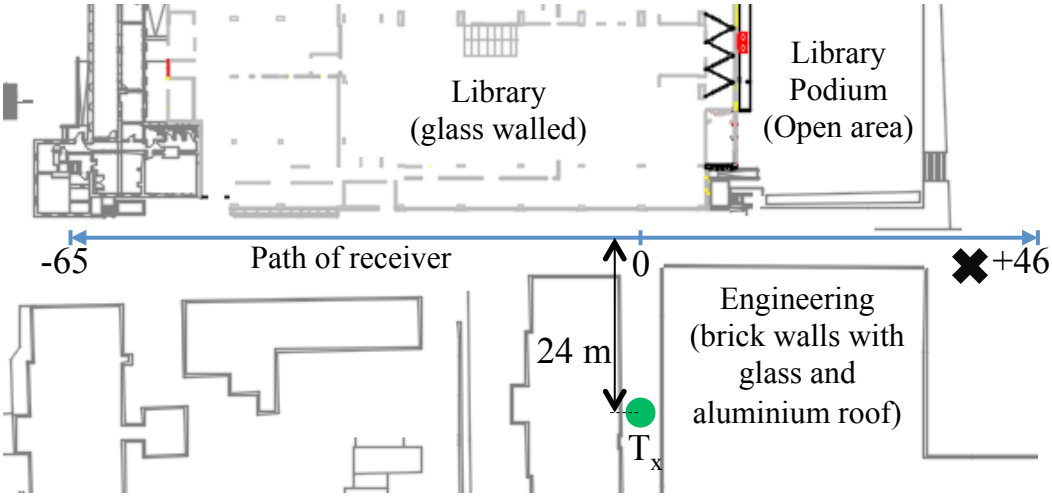

Figure 4. Map of Junction A indicating the location of the transmitter and the path of the receiver.

For each junction, the transmitter was fixed in position (as indicated in the figures – note that two transmitter positions, 50 m and 70 m from the junction, were used for Junction B). Measurements were then collected by the stationary receiver at various distances, d_r from the center of the junction separated by fixed intervals (Δd). A laser-rangefinder was used to determine the location of the transmitter and receiver relative to a fixed reference point (the nominal center of each junction) with an accuracy of ±0.5 mm. For Junction A, Δd =1 m, while for Junctions B and C, Δd=0.2 m. The separation between measurement points (Δd) was a compromise between

practicality (i.e. the time taken to complete the measurements) and having a resolution sufficient to observe the fading.

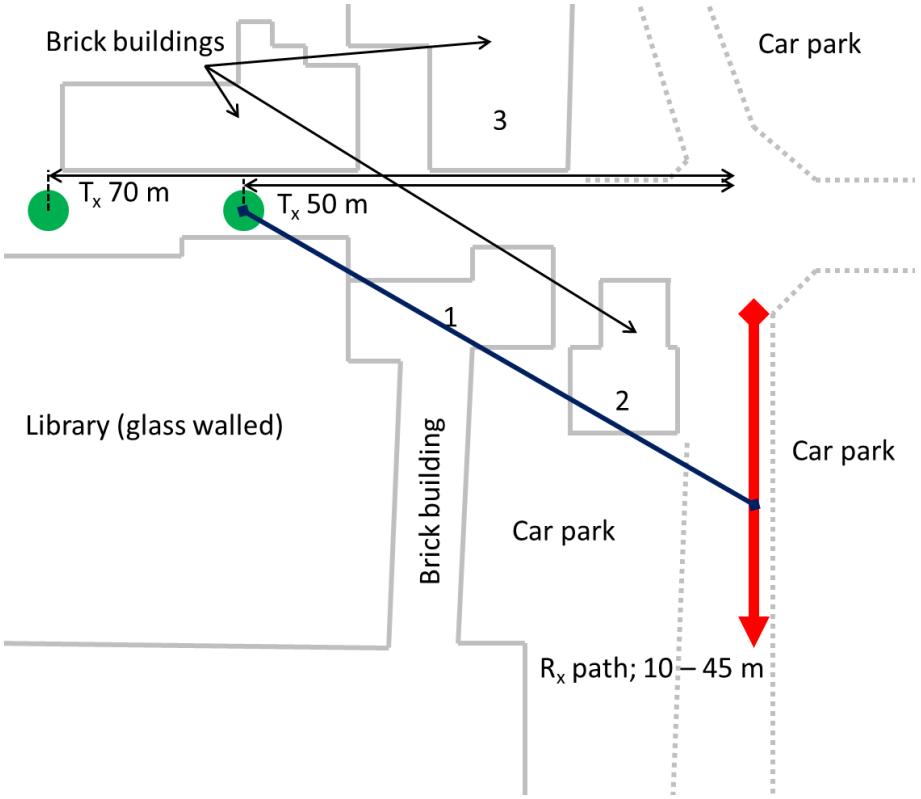

Figure 5. Map of Junction B. Two positions, 50 and 70 m from the junction, were used for the transmitter. A direct line from Tx50 to d_r=30 m is also marked.

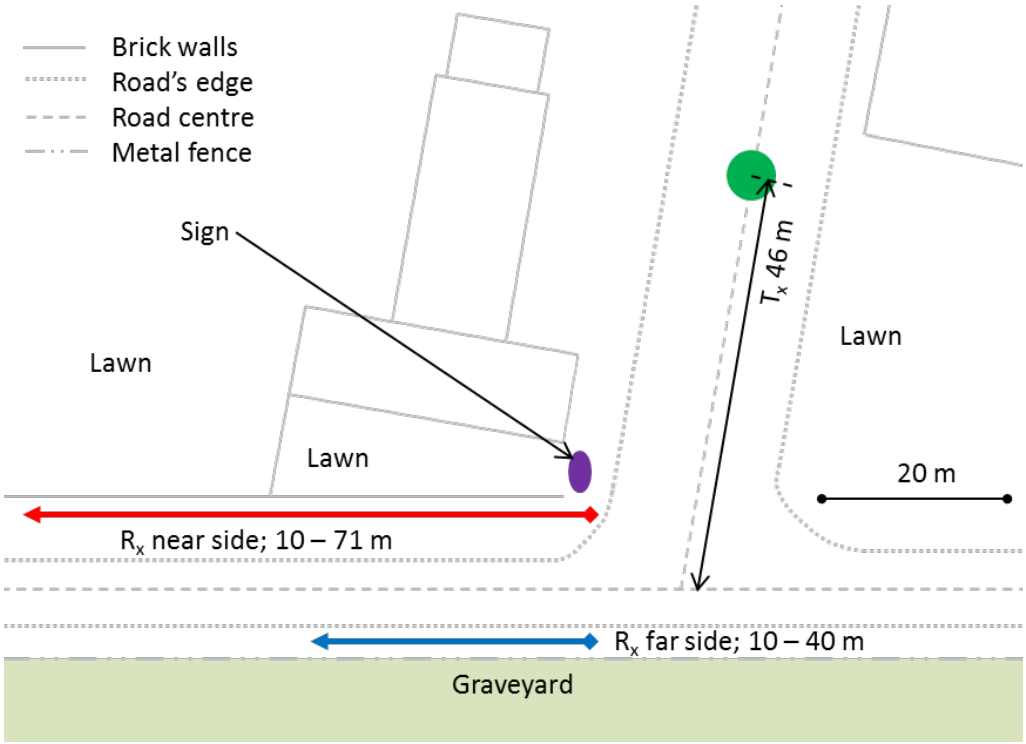

Figure 6. Map of Junction C

3 Results

3.1 Junction A

Junction A is relatively built-up with buildings located along all roadsides (Figure 4). However, the buildings are not uniformly distributed on either side of the junction since it is more open in the positive d_r direction (e.g. the Library Podium is an open space on a raised platform with 1.68 m high walls). The transmitter was placed in the center of a 4.7 m wide street canyon a distance 24 m from the junction, while the receiver moved along the middle of the road either side of the T-junction from −65 m to 46 m. The receiver was located within line-of-sight (LOS) of the transmitter in six positions ($-3.2<d_r<3.1$ m) with the remainder being non-line of sight (NLOS). Measurements were taken during a series of six separate runs with some overlap in d_r between the runs. While there are some differences in behavior between runs, the general trends are the same and therefore the results from the different runs have been combined.

The observed MPP and PDR from all six runs as a function of d_r are presented in Figure 7. As expected, both the MPP and PDR are high at the center of the intersection, in the LOS region, and decrease with increasing $|d_r|$. The MPP exhibits fading (of up to 10 dB) even in the LOS region, indicating that multipath propagation is likely to be present. The inter-decile range of MPP for each location tends to be higher during deeper fades providing additional evidence that multipath is present. The reduction in MPP and PDR is more marked in the positive d_r direction than for negative d_r. This may arise because there are buildings on both sides of the road at negative d_r that will reflect the radio waves and extend the coverage range, while for d_r >10 m, there is a building on only one side of the road, and this will reduce the number of reflections and hence the signal strength. There is reasonable agreement between the observations and the various models in the LOS region, but generally very poor agreement in the NLOS regions. This indicates that the principle mechanism by which the signal is propagating into the NLOS region is not diffraction. For penetration through the building, the so-called standard or default parameters reported by Sommer et al. (2011), i.e. β~9 dB and γ~0.4 dB/m, lead to a received signal power generally significantly below that observed. Fitting the model curve to the observations, by definition, provides good agreement, but with fitted parameters of β~0.45 dB and γ~0.4 dB/m for the building to the left of the junction and β~0.0 dB and γ~0.6 dB/m for the building to the right of the junction, it is evident that the attenuation per wall is significantly lower than those measured by Sommer et al. (2011) even for lightly constructed buildings, whereas the buildings in the experiments described here are brick-built (left hand side) and constructed of aluminum, glass, and brick (right hand side). This evidence strongly suggests that the contribution to the overall signal received directly through the building is likely to be small. The disagreement between the observations and virtualsource11p arises because this junction is significantly different from those used to derive this model. For example, w_r (8.5 m) and d_t (24 m) are below the minimum values of 20 m and 30 m, respectively, used by Mangel et al. (2011). In addition, the junction is a T-junction and not a crossing street and this will increase the received power since the some of the transmitted signal will reflect from the building opposite the T rather than being lost into an additional leg of the junction. From the measurements of PDR, three regions can be identified. From $-20<d_r<10$ m, the network operates with close to 100% reliability, for d_r <−55 and d_r >40 m, the network operates with close to 0% reliability (although for some positions the PDR is higher than this), while between these two cases lies a transition region with strongly varying PDR. The maximum range by road between transmitter and receiver for which the PDR>90% (Meireles et al, 2010), R_{max} is about 45 m (d_r~21 m and distance from transmitter to junction is 24 m).

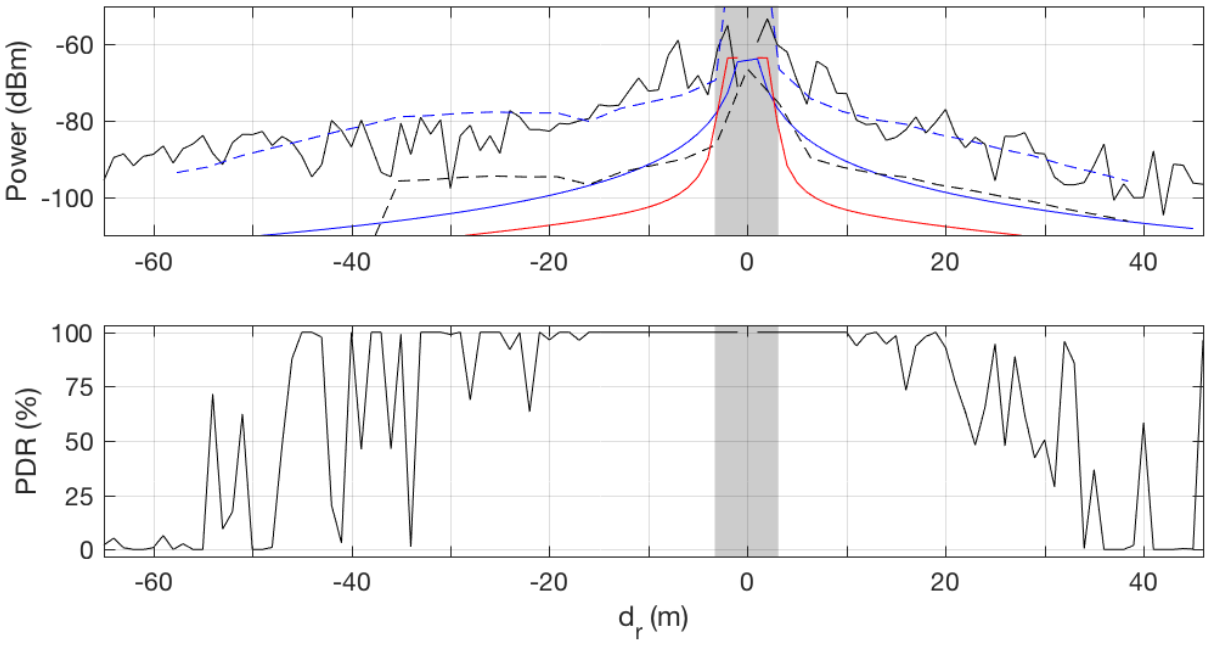

Figure 7. Plot of (top panel) median peak signal power and (bottom panel) PDR as a function of distance from the intersection for Junction A. The solid blue line is the virtualsource11p prediction of the received power for the urban case while the red line is knifeedge diffraction. The dashed lines are for the model of Sommer et al. (2011) with standard (black) or fitted (blue) parameters. The shaded area represents where a LOS path is present. Error bars are omitted for clarity, but the inter-decile ranges in power are typically 5 dB (a similar value to that observed by others, e.g. Tchouankem et al., 2015).

3.2 Junction B

The area around Junction B is less-built up than for Junction A (see Figure 5). While the transmitter was placed in a street canyon, the road along which the receiver was moved had buildings only on one side and an open area (a car park) lined with a hedge on the other and was wider than for Junction A. For this experiment, because of higher volumes of traffic, the transmitter was placed on and the receiver moved along the pavements at the edge of the road instead of the center of the road.

Two sets of measurements were made, the first with the transmitter 50 m away from the junction center (Tx50) and a second 70 m away (Tx70). In both cases, measurements were made with Δd=0.2 m and, since it was not possible to safely conduct measurements at d_r <10 m, the geometry meant that NLOS conditions were present throughout. Limitations in the battery life of the equipment meant that these measurements were obtained over a period of four days with small overlaps in d_r between successive runs. As for Junction A, measurements made at the overlapping distances were similar indicating that changes in the propagation environment from day to day (e.g. the location of parked cars) had minimal effect, and therefore the results were combined. During these experiments, a partial manual record was made of the road vehicle traffic that was occasionally present and visible from the receiver location.

The observations of MPP and PDR for Tx50 and Tx70 are presented in Figure 8. As expected, the signal strength tends to decrease with increasing d_r, although both spatial and temporal fading is of the order of 6 dB and there are peaks in the signal that do not appear to be well related to any changes in the propagation path (e.g. when d_r ~30 m with Tx50 there is no obvious change in the propagation environment that leads to the increase in signal strength, see Figure 5). The converse is also true since there is no obvious effect on the signal strength for Tx50 when the direct path between the transmitter and receiver enters the shadow of the library at

d_r~13 m or comes out of the shadow of Building 2 at d_r ~34 m. The level of the signal arriving at the receiver having propagated through the buildings assuming the standard parameters reported by Sommer et al. (2011) is significantly below that observed. As for Junction A, the best-fit value of β~0.0 dB (note that γ~0.8 dB/m) indicates that there is no loss associated with the building walls and therefore, together with the poor agreement in the behavior of the best fit curve with the observed values suggests that building penetration is not the dominant mechanisms for this junction. This is also the case for diffraction since the calculated signal levels are below those observed. This can be contrasted with the generally a good agreement between the observations and virtualsource11p, particularly when d_t=70 m. Although this junction lacks buildings on the far side of the road, the larger values of w_r and d_t together with the presence of four legs at the junction ensure that the behavior is closer to that of the junctions studied by Mangel et al. (2011). Experimentally there is a mean difference of 1.4 dB between the received power for Tx50 and Tx70 in the range 10<d_r<45 m (the standard deviation is 6 dB), which is smaller than the difference of 3.8 dB derived from virtualsource11p.

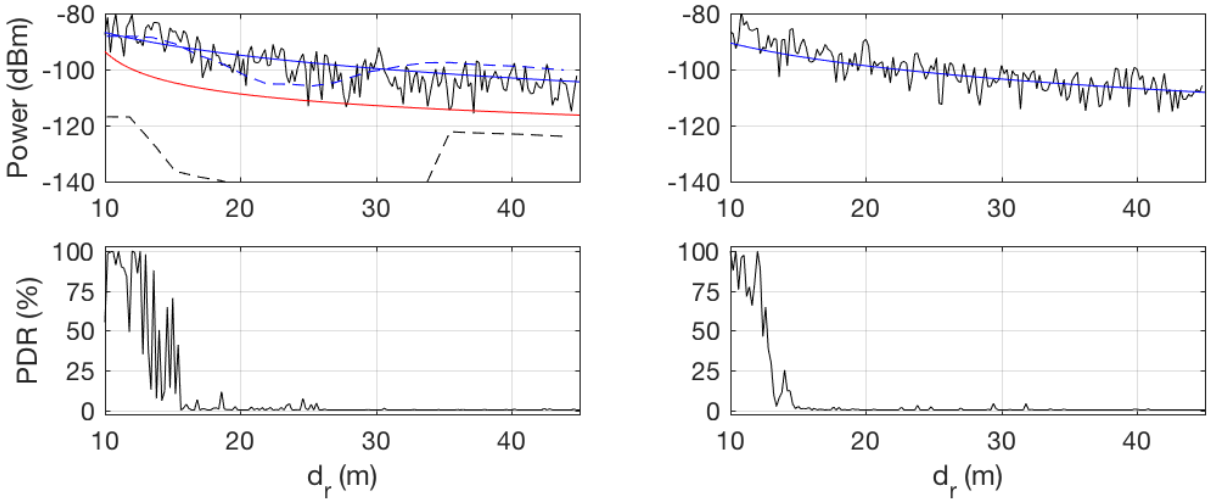

Figure 8. As for Figure 7, except for Junction B (left hand panels are for Tx50 and the right hand panels for Tx70). Note that propagation was non-LOS at all distances. The interdecile range of the power was approximately 6 dB.

For both Tx50 and Tx70, there is a strong reduction in PDR coupled with a gradual decline in signal strength as d_r increased from 10 m to approximately 15 m. The boundary between where PDR=100% and where PDR=0% is much sharper for Tx70 than for Tx50. R_{max} is difficult to determine for Junction B, since measurements were not taken for d_r<10 m and the PDR is already less than 90% at that distance for Tx50. When d_r>15 m for Tx50, the signal strength continues to reduce while the PDR is largely zero except for a few, relatively small, peaks that are strongly related to the presence of vehicles. For example, for Tx50 there is a peak in the PDR of 12% at d_r=18.6 m (Figure 8) that coincides with the passage of a truck through the intersection. At d_r=21.2 m an SUV passed but only had a marginal effect on the PDR. An increase in traffic was noted at d_r=23.4 m and this has given rise to an increase in the PDR to 2.8% but did not affect the MPP. At d_r=24.6 m the PDR increases to ~7% although no vehicle was noted manually. However, the results presented in Figure 9 indicate that there were two intervals (at times of 20 s and 35 s) of increased Doppler spread that accompanied this increase in the PDR. In the first interval, there is also a small (~4 dB) increase in the peak power accompanying one of the peaks in PDR, but no increase with the other, while in the second interval a strong increase in peak power occurs. Care must be taken when comparing the results derived from the 802.11p devices and those derived from the spectrum analyzer since the spectra are produced over a much longer time (~1.5 s) than the packets (0.1 s) and therefore rapid changes in the propagation environment will not necessarily be reflected in the spectrum.

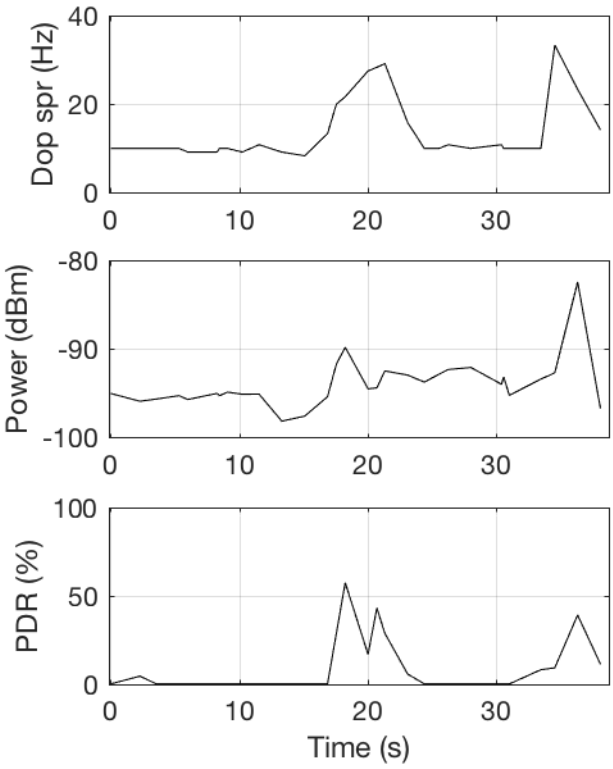

Figure 9. Plot of (from top to bottom) Doppler Spread, peak power, and PDR as a function of time for Junction B at d_r=24.6 m with Tx50. The PDR is calculated per spectrum (i.e. based on ~15 packets in 1.5 s).

The measurements taken for d_r>18 m with Tx50 (i.e. the region where the PDR is generally 0) have been categorized by whether the PDR is zero (102 out of 135 measurements) or non-zero (33 cases). For each case, the data have been further categorized into whether a vehicle is present or not. Whether a vehicle was present has been determined from either the manual record or where the Doppler spread has been increased (e.g. Figure 9). The outcome from this analysis is presented in Table 1. Several conclusions can be drawn from these results:

1. Where the PDR is non-zero there is almost always a vehicle present (the one exception is for d_r=20.8 m)
2. The presence of a vehicle does not always increase the PDR (about 29% of the cases where a vehicle is present leaves the PDR unchanged)

Table 1. The number of events in each category (the percentage is indicated in brackets) for measurements made at Junction B for d_r>18 m and Tx50

	Non-zero PDR	PDR=0
Vehicle present	32 (23.7)	13 (9.6)
No vehicle	1 (0.7)	89 (65.9)

3.3 Junction C

The layout of Junction C together with the location of the transmitter and the two paths taken by the receiver are presented in Figure 6. The transmitter was fixed at the center of a four-lane road at a distance of 46 m from the center of the intersection. Measurements were taken along the sides of the road 5 m from the center on the same side as the junction (referred to as ‘near side’) and 8 m from the center on the far side with Δd=0.2 m. This junction is open compared to the others with a building present only to one side (i.e. there were no street canyons). There was a mix of LOS and NLOS conditions on both paths with data being collected over 10 m into the NLOS region on the far side and over 50 m into the NLOS region on the near side. A road sign blocks the visible LOS when d_r~25 m and d_r~19 m for the far and near side paths, respectively. The plastic

construction of the sign means that it should not have a significant effect on the radio propagation or network performance. A wall lies along the near side path and as the path slopes downwards away from the junction, the height of this wall relative to the path increased. On the far side, there was an iron railing fence between the path and the graveyard that is likely to have reflected some of the radio waves.

The PDR and MPP for the data collected on the far and near side paths are presented in Figure 10. For both paths, the PDR is close to 100% for d_r<25 m and for the near side, when d_r>40 m, the PDR is highly variable lying between 0 and close to 100%. R_{max} is approximately 70 m for both the near-side and far-side cases. As expected, the MPP tends to reduce with distance although it exhibits fading of about 8 dB. As with Junction B, the diffracted signal does not make a significant contribution to the overall signal power, while there is a good agreement between virtualsource11p and the observations. Again, like Junction B, this junction is more reminiscent of those reported in Mangel et al. (2011) and therefore it is unsurprising that there is agreement. It is noteworthy that, as mentioned above, the metal fence may be a strong reflector of the signal and therefore forms the street canyon. An interesting result is that for the far side, the MPP in the LOS region just after the road sign (d_r~25 m) is about 5 dB higher than in the NLOS regions either side. In addition, the MPP in this LOS region is marginally higher than that in the LOS region just before the road sign (i.e. for d_r between 20 and 22.60 m). This is a systematic effect (i.e. it is not related to traffic) since the majority of the spectra taken in this region exhibit increased power and the variation in signal power is low compared to far side observations at other d_r. The corner of a building starts to obscure the LOS at positions just beyond this region (see Figure 6) and therefore the geometry means that it is likely that reflections from the building are leading to the increase in MPP. The effect of the building on the signal power measured on the near and far sides is demonstrated in Figure 11. Three regions can be identified: 10–15 m where the power is approximately the same on both sides of the road and both paths are LOS; 15–26 m where the near side path is in the shadow of the building and, consequently, exhibits lower signal power; and for 26 m and greater where both paths are NLOS and the MPP on the far side decreases.

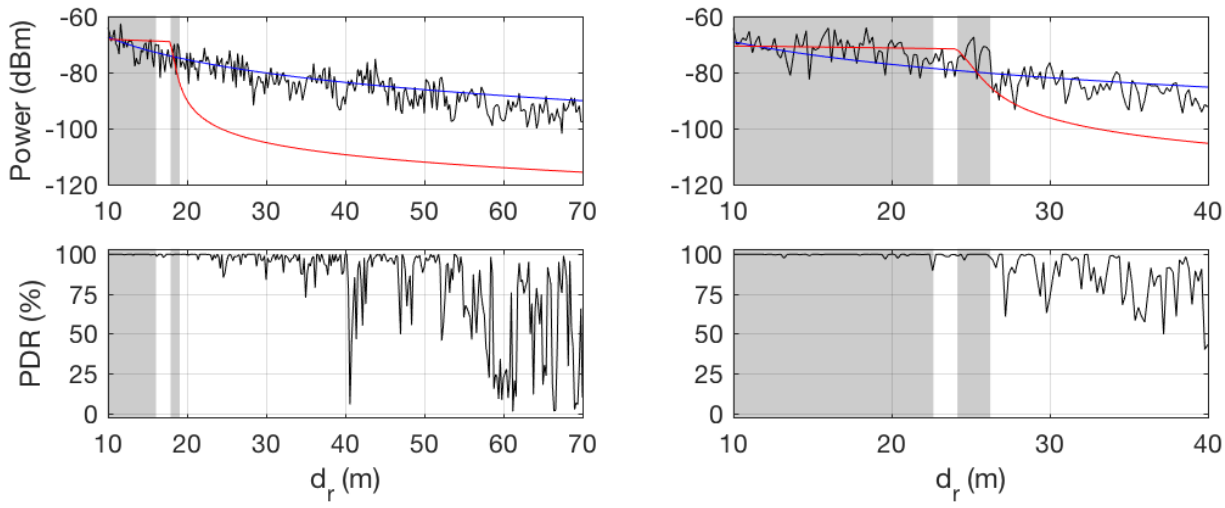

Figure 10. As for Figure 7, except for Junction C, (left hand column) near side and (right hand column) far side. The interdecile range of the power was approximately 8 dB for both near and far sides.

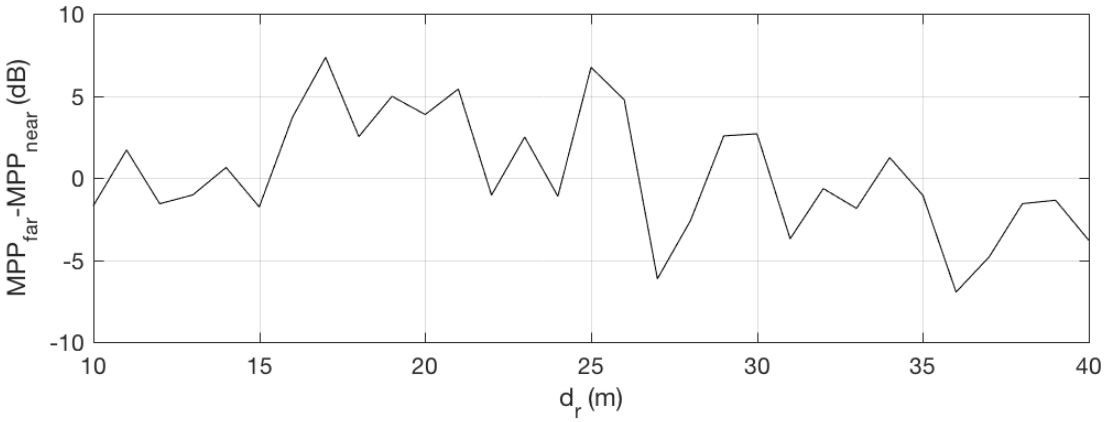

Figure 11. The difference in the MPP measured on the far and near sides of Junction C as a function of distance from the junction (the MPP have been averaged in bins 1 m wide).

3.4 Network performance as a function of signal strength

The behavior of the mean PDR observed in MPP bins 1 dBm wide for all experiments is presented in Figure 12. Three regions of behavior can be identified, for MPP>–75 dBm, PDR is close to 100%, for MPP<–105 dBm, PDR=0%, while between these there is a transition region where the PDR tends to increase with increasing signal strength. A best fit sigmoid curve of form

$$PDR(\%) = \frac{100}{1+10^{a(b-P)}} \quad (3)$$

has also been plotted, where P is the power (in dBm) and the fit parameters are a=0.104 and b=–91.5 dBm. While this type of performance curve will be useful for modelers to obtain typical values of PDR from a calculated value of the received signal strength, it should be remembered that this curve has been derived for a particular model of 802.11p network node operating at a data rate of 6 Mbps, for situations where the Doppler shifts and spreads are relatively low, and where there is no contention for the channel. It is useful to note that the results bear some similarity to the uncalibrated laboratory measurements of packet error rate reported by Sjöberg et al (2010) and suggests a receiver sensitivity of approximately –95 dBm.

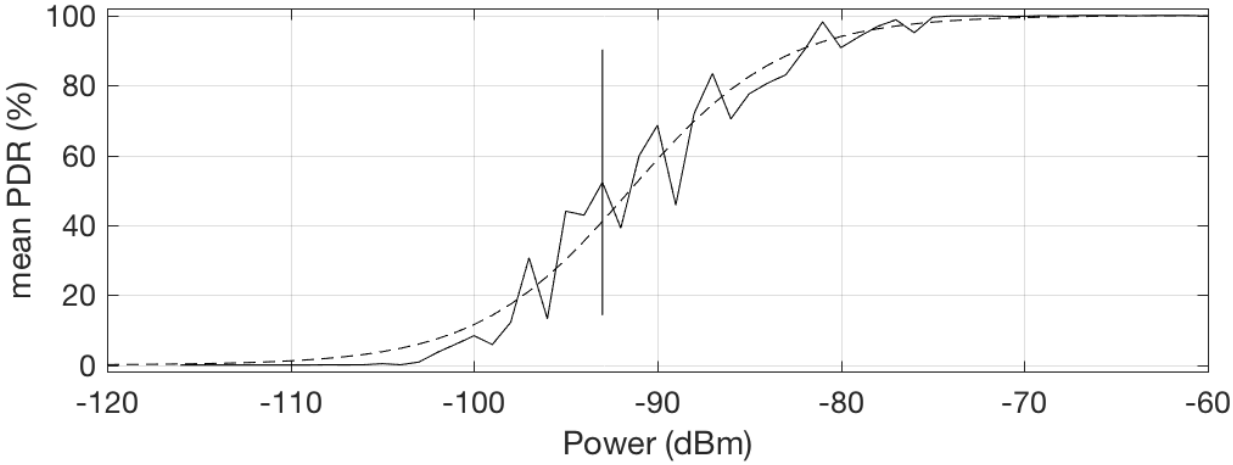

Figure 12. Plot showing the relationship between the average PDR and MPP for all observations. The MPP is binned into integer values of dBm. The typical inter-decile range in the transition region between good and poor performance is indicated as an error bar (the inter-decile range in the good and poor regions is a few percentage points). The dashed line is a best fit sigmoid curve.

4 Concluding remarks

In this work, we have measured the signal characteristics and network performance of 802.11p systems at three road junctions representative of those found in the urban environment. Given the approach adopted in the experiments reported here, some care should be exercised in interpreting the results in the context of V2V or V2X scenarios. For example, the height of the antennas (about 1 m from ground level) is lower than that found for a roof mounted antenna on a typical car (~1.5 m) or small van (~2 m) and the antennas do not have a ground plate. However, antenna heights are not included in the models discussed here, except for virtualsource11p where it appears in the value of the breakpoint (d_b~79 m for h_t=h_r=1 m). Measurements presented in supporting information Figures S1 and S2 indicate for Junction A that changing the height of the transmitter has a strong effect on the received signal at values of d_r within, or a few metres beyond, the LOS region, but little effect at greater distances. The addition of a metal ground plane with h_t=1 m or placing the antenna on the roof of a van (h_t=2 m) has a similar effect to changing the height (see supporting information Figure S3). Another possible source of divergence of the experiments reported here from vehicle mounted antennas is that some antennas proposed for use in V2V are directional and when positioning omnidirectional antennas on the roof of a vehicle, the geometry of the roof, or roof furniture (e.g. roof racks) may result in a non-uniform radiation pattern (e.g. Kwoczek et al., 2011). Given the rich multipath environment, an antenna with directional characteristics will excite the channel quite differently to an omnidirectional antenna and hence the behavior of the received signal power may be different to that reported here.

Given the caveats discussed above, the observed range for reliable operation, R_{max} (defined as the maximum range for which PDR>90%) was dependent on the junction but lay in the range 45–70 m which is consistent with those values found by Meireles et al. (2010) and Schumacher et al. (2012). How much time this then affords collision avoidance systems depends on the speed and the stopping distance achievable with the road surface and vehicle condition. For example, at 48 km/h, the minimum stopping distance (i.e. under good road conditions and with a well-maintained vehicle) is approximately 14 m (Department for Transport, 2015). Given two vehicles approaching each other at this speed and detecting each other at a range of 45 m, this would leave a ‘thinking distance’ of 17 m and therefore a processing time of 1.3 s. For manually driven cars, the ‘thinking distance’ would be about 18 m (which assumes drivers who are alert and concentrating) and therefore a low speed collision would occur. An interesting result is that the presence of vehicles at Junction B led to an improvement in the PDR in about 70% of cases, which can be contrasted with the usual expectation that vehicles will cause additional shadowing (e.g. Meireles et al., 2010). However, it is important to note that the effect of the vehicles on the PDR is small (up to about 50% over a few seconds, but only 7% over 30–45 seconds) and will not enable reliable communications.

While virtualsource11p provides an excellent agreement to the measurements for appropriate cases (i.e. where the junction layout matches those used in deriving virtualsource11p), there is poor agreement with the measurements for a junction that deviates in form too far from those used to derive virtualsource11p. This demonstrates one of the weaknesses of using parameterized empirical models for complex propagation environments. The building shadowing model of Sommer et al. (2011) has also been applied in two cases. Using typical building parameters (i.e.β ~9 dB and γ~0.4 dB/m), the model results underestimate the signal strength for Junction A, while, for Junction B, no effect on the signal strength was observed at distances where the path left the shadow of a building although a strong increase was predicted by the shadow model. Best fitting the model to the observations presented here results in a very low value of wall attenuation (i.e. β<0.45 dB) for both junctions that, given the solid construction of the buildings, is not physically realistic. Therefore, for the situations reported here, the signal on paths through buildings was weak compared to the reflected signal. This was also the case for the diffracted signal at each junction.

The measurements reported in this paper have also allowed the received signal strength to be linked with the resultant network performance (i.e. PDR). While there are some limitations in the applicability of the expression derived from the observations (e.g. there was no contention for the channel during the experiments), it will be useful in providing a simple method to find the network performance based on the results from propagation modelling.

Acknowledgements

The authors would like to thank Horiba-MIRA for the loan of the network system. The experimental measurements reported in this paper are included in the supporting information.

References

Abbas, T., Thiel, A., Zemen, T., Mecklenbräuker, C.F., & Tufvesson, F. (2013). Validation of a non-line-of-sight path-loss model for V2V communications at street intersections. In *2013 13th International Conference on ITS Telecommunications (ITST)*. IEEE, pp. 198–203.

Alexander, P., Haley, D., & Grant, A. (2011). Cooperative Intelligent Transport Systems: 5.9-GHz Field Trials. *Proceedings of the IEEE*, 99(7), pp.1213–1235.

Cheng, L., Henty, B.E., Stancil, D.D., Bai, F., & Mudalige, P. (2007a). A fully mobile, GPS enabled, vehicle-to-vehicle measurement platform for characterization of the 5.9 GHz DSRC channel, In *IEEE Antennas and Propagation Society, AP-S International Symposium (Digest)*. pp. 2005–2008.

Cheng, L., Henty, B.E., Stancil, D.D., Bai, F., & Mudalige, P. (2007b). Mobile Vehicle-to-Vehicle Narrow-Band Channel Measurement and Characterization of the 5.9 GHz Dedicated Short Range Communication (DSRC) Frequency Band. *IEEE Journal on Selected Areas in Communications*, 25(8), pp.1501–1516.

Department for Transport (2015). The Highway Code. U.K. government

ITU-R (2018). P.526-14, Propagation by diffraction, International Telecommunications Union, Geneva.

Jiang, D., Chen, Q., & Delgrossi, L. (2008). Optimal data rate selection for vehicle safety communications. In Proceedings of the fifth ACM international workshop on VehiculAr Inter-NETworking - VANET '08. New York, New York, USA: ACM Press, p. 30.

Kwoczek, A., Raida, Z., Láčík, J., Pokorny, M., Puskelý, J., & Vágner, P. (2011). Influence of Car Panorama Glass Roofs on Car2Car Communication, IEEE Vehicular Networking Conference (VNC). IEEE, Nov. 2011, pp. 246-251, DOI: 10.1109/VNC.2011.6117107.

Mangel, T., Klemp, O., & Hartenstein, H. (2011), 5.9 GHz inter-vehicle communication at intersections: a validated non-line-of-sight path-loss and fading model. *EURASIP Journal on Wireless Communications and Networking*, 2011:182.

Meireles, R., Boban, M., Steenkiste, P., Tonguz, O., & Barros, J. (2010). Experimental Study on the Impact of Vehicular Obstructions in VANETs, *Proc. IEEE Vehic. Net. Conf. (VNC)*, pp. 338-45.

Paier, A., Tresch, R., Alonso, A., Smely, D., Meckel, P., Zhou Y., & Czink, N. (2010). Average downstream performance of measured IEEE 802.11p infrastructure-to-vehicle links, in *IEEE*

International Conference on Communications, Workshop on Vehicular Connectivity, Cape Town, South Africa.

Pilosu, L, Fileppo, F., & Scopigno R. (2011). RADII: A Computationally Affordable Method to Summarize Urban Ray-Tracing Data for VANETs, 2011 7th International Conference on Wireless Communications, Networking and Mobile Computing, DOI: 10.1109/wicom.2011.6040412.

Schumacher, H, Tchouankem, H., Nuckelt, J., Kürner, T., Zinchenko, T., Leschke, A., & Wolf, L. (2012). Vehicle-to-Vehicle IEEE 802.11 P Performance Measurements at Urban Intersections, *IEEE International Conference on Communications* (ICC), pp. 7131-7135.

Sjöberg, K., Kåredal, J., Moe, M., Kristiansen, Ø., Søråsen, R., Uhlemann, E., & Ström, E. (2010). Measuring and using the RSSI of IEEE 802.11p. Paper presented at *17th World Congress on Intelligent Transport Systems* (ITS), Busan, Korea, Republic of.

Sommer, C., Eckhoff, D., German, R., & Dressler, F. (2011). A computationally inexpensive empirical model of IEEE 802.11p radio shadowing in urban environments. In *Eighth International Conference on Wireless On-Demand Network Systems and Service*s. IEEE, pp. 84–90.

Tchouankem, H., Zinchenko, T., & Schumacher, H. (2015). Impact of Buildings on Vehicle-to-Vehicle Communication at Urban Intersections. *12th Annual IEEE Consumer Communications and Networking Conference* (CCNC), pp. 206-212.